Kinetics of x-ray lasing by resonant photoexcitation: Fundamentals of pumping power and gain for the Na X—Ne IX system

J. P. Apruzese and J. Davis
Plasma Radiation Branch, Code 4720, Plasma Physics Division, Naval Research Laboratory, Washington, D.C. 20375-5000
(Received 30 November 1984)

Two of the most fundamental aspects of the sodium-neon resonantly photopumped x-ray laser system are examined: the functional dependencies of the sodium-plasma pumping-line power output and the atomic-level kinetics in the neon which determine gain. For sodium, the growth of pumping power with size, temperature, and density of the plasma is quantified with numerical and analytic calculations. In the neon an analytic model of the gain kinetics is developed which allows quantitative assessments of the effects of each important rate and process on the gain. Both analytic models should be applicable to similar resonantly pumped systems by using the appropriate rates for those systems. In addition, a novel way of depleting the lower lasing state in an optically thick laser medium is presented.

I. INTRODUCTION

About a decade ago it was suggested[1,2] that population inversions in highly ionized plasmas could be obtained by radiative pumping of closely matched lines from different elements or different ionization stages of the same element. Some experimental success[3,4] has been achieved in inverting the $n=4$ and $n=3$ levels in Mg XII and Mg XI by pumping with resonant Ly-α and $1s^2-1s2p\ ^1P$ transitions in C VI and C V. More recently, enhanced ultraviolet fluorescence has been demonstrated[5] using matched-line pumping of C II by Al III. Quite a few other promising matched-line pairs have been identified.[1,2,6–9] In evaluating the practicality of any of the matched-line schemes, one must first be concerned with the level of pumping photon flux which can be obtained with a given plasma. In general, the greater the pumping flux, the larger the achievable gain in the pumped plasma. Delineating the relationship of various pumping-plasma properties to the achieved output power is a principal subject of this paper. Also of great importance to the viability of this technique are the essentials of the level kinetics in the pumped plasma. This determines the actual gain in conjunction with the impinging photon flux. We show below that it is possible to develop analytical parametrizations for the photon transport of the pumping radiation as well as the kinetics of the gain medium. These analytic models exhibit clearly the influence of all the important plasma and atomic parameters. They are also useful for quantitative assessments.

In this paper we consider one of the most promising of the proposed systems: the Na X $1s^2\ ^1S_0-1s2p\ ^1P_1$ line at 11.0027 Å pumps the Ne IX $1s^2\ ^1S_0-1s4p\ ^1P_1$ line at 11.0003 Å. The strongest potential lasing lines in the pumped neon plasma are $2p\ ^1P_1-3d\ ^1D_2$, $2p\ ^1P_1-4d\ ^1D_2$, and $3d\ ^1D_2-4f\ ^1F_3$. The attractiveness of this scheme stems from several features. Both ions are heliumlike, a closed-shell configuration which is present over a relatively wide range of plasma conditions. The line wavelength match is excellent—two parts in 10^4—which is about one Doppler width. Also, both ions are readily producible in either laser plasmas or Z pinches driven by high-power pulsed generators. In previous work[10] we have demonstrated that substantial power in the sodium line was achieved in a laser-fusion implosion experiment at Rochester[11] in which sodium impurities were unintentionally included in the glass microballoon. In this experiment a brightness temperature of 227 eV was achieved in the pumping line. No numerical modeling of the sodium was possible since the impurity concentration was unknown. The line intensity was obtained by modeling the neon spectrum emitted by the compressed microballoon, and inferring the sodium-line intensity from its strength relative to the modeled neon lines. The neon model was used[10] to numerically demonstrate that temperatures of 50—100 eV and electron densities of $10^{19}-10^{20}$ cm^{-3} in the neon component would produce substantial gains when exposed to the 227 eV sodium radiation. In Sec. II, an analytic model of the Ne IX kinetics is developed which has been found to reproduce in considerable detail and to clarify the previous numerical results. In Sec. III, a numerical atomic model of the pumping sodium-plasma component is detailed, and quantitative results of the power output in the pump line are given as a function of the basic plasma properties. An accurate analytic parametrization is developed for the pump-line photon transport which greatly influences the power output.

II. BASIC KINETICS OF THE PUMPED NEON PLASMA

Even though contiguous sodium-neon components will ultimately influence each other's properties, it has been found possible to minimize this by use of a transparent thermal buffer separating them.[12] It is useful conceptually, and reasonable physically, to consider the neon plasma separately and characterize its interaction with the sodium solely by its absorption of a given pumping-line flux. Let us assume this flux is impinging from one side—i.e., it fills 2π steradians. If T(eV) is the effective brightness temperature of the sodium line, the associated net flux, as-

suming isotropic emission from the illuminated 2π steradians, and that $T \ll 1127$ eV, is

$$\mathcal{F}_\nu = 2\pi \int_0^1 B_\nu(T)\mu\, d\mu = \pi B_\nu(T) \simeq 9.4\times 10^5 e^{-(1127\text{ eV})/T} \text{ ergs/cm}^2\text{ sec Hz}, \quad (1)$$

where in Eq. (1), μ is the cosine of the ray angle. The projection factor $\mu=\cos\theta$ averaged over the hemisphere reduces the net directional flux $\pi B_\nu(T)$ by a factor of 2 from the angle integrated specific intensity $2\pi B_\nu(T)$. Although it is the net flux which is usually measured in the laboratory, the pumping rate is independent of the angle at which the photons flow. Therefore the equivalent pumping rate per neon ion in the heliumlike ground state is

$$P_4 = \int_{-\infty}^{+\infty} \frac{2\pi B_\nu(T)}{h\nu}\sigma_\nu d\nu \text{ sec}^{-1}, \quad (2)$$

where σ_ν, the cross section for photoabsorption in the Ne IX $1s^2$–$1s4p\ ^1P$ line is given by

$$\sigma(\nu) = \frac{\pi e^2}{mc} f\phi(\nu). \quad (3)$$

In Eq. (3), f is the line absorption oscillator strength (0.056) and $\phi(\nu)$ is the normalized-line profile. Our calculations show that sodium-line fluxes intense enough to pump significant inversions in the neon arise from sodium plasmas optically thick enough to cause substantial opacity broadening and saturation in the emitted-line profile. Therefore we may reasonably assume that the sodium flux is constant across the absorption profile of the Ne IX $1s^2$–$1s4p\ ^1P$ line. Hence

$$P_4 = \frac{2\pi B_\nu(T)}{h\nu}\frac{\pi e^2}{mc} f \text{ sec}^{-1}, \quad (4)$$

where T refers not to the kinetic temperature of the sodium plasma but the equivalent blackbody temperature of the pumping Na X $1s^2$–$1s2p\ ^1P$ line. Inserting the appropriate numerical values in Eq. (4) leads to

$$P_4 = 1.54\times 10^{12}\, e^{-(1127\text{ eV})/T} \text{ sec}^{-1}. \quad (5)$$

For an equivalent flux temperature of 227 eV, as found in the Rochester experiment,[10,11] Eq. (5) yields a pumping rate P_4 of 1.1×10^{10} sec^{-1} for the $1s4p\ ^1P$ level of Ne IX per ground-state neon ion. At the highest neon-plasma temperature conducive to substantial gain[10] (~ 100 eV), the collisional excitation rate coefficient $1s^2$–$1s4p\ ^1P$ is 2×10^{-16} cm^3 sec^{-1}. The highest ground-to-excited collisional rate coefficient is to the $1s2p\ ^1P$ level (1.4×10^{-14} cm^3 sec^{-1}). At electron densities of 10^{20} cm^{-3}, these rates are equivalent to pumping of 2×10^4 sec^{-1} and 1.4×10^6 sec^{-1}, far below any reasonably achievable sodium photon-pumping rate. Recombination rates to form the Ne IX excited states depend upon the Ne X fraction. However, for a plasma which is half hydrogenlike and half heliumlike, with $N_e = 10^{20}$ cm^{-3}, the highest collisional and radiative recombination rates at 100 eV are 2 orders of magnitude below the photon-pumping rate quoted above. Thus, in a properly prepared sodium-neon system, excited-state population of the neon levels is dominated by the pumping photons. This fact provides the basis for the analytic description below.

In the following equations, numerical subscripts refer to the singlet levels of Ne IX. For convenience the ground-state population $N(1s^2\ ^1S_0)$ is set to unity. With this convention, the creation rate of the $n=4$ singlets is given by P_4, exactly as in Eq. (5). The D's refer to the destruction rate of the level, i.e., the sum of all the collisional and radiative rates out of the level. F_i is the fractional population (relative to the ground state) of level i. The singlet sublevels are assumed to be statistically distributed and the justification for this assumption is the agreement the model produces with previous numerical results.[10] Equilibration time of the excited states relative to the ground state is controlled by the spontaneous decay rates, which greatly exceed the collisional deexcitation rates at densities suitable for gain ($N_e < 10^{21}$ cm^{-3}). The equilibrium time is approximately A^{-1} where A is the spontaneous decay rate. Averaged over the $n=4$ singlet sublevels, A^{-1} equals 5 psec. Therefore the steady-state assumption provides a reasonably accurate description of level populations in these plasmas whose hydrodynamic time scales are at least an order of magnitude larger. In steady state, the fractional population is equal to the creation rate divided by the destruction rate, i.e.,

$$F_4 = P_4/D_4. \quad (6)$$

The $n=2$ and $n=3$ singlet levels are ultimately controlled by the pumping of $n=4$. As shown above, coupling upward from the ground state is negligible. However, radiative decay to the ground state is very important. Let C_{ij} and A_{ij} stand for the collisional rate coefficients and radiative rates coupling the $n=i$ and $n=j$ singlet levels, respectively. The $n=4$ level is the highest level which need be considered when radiative population of this level dominates the kinetics. Define

$$R_{ij} = C_{ij}N_e + A_{ij} \text{ sec}^{-1}, \quad (7a)$$

$$D_i = \sum_{j=1}^{4} C_{ij}N_e + A_{ij} \text{ sec}^{-1}. \quad (7b)$$

The $n=2$ and $n=3$ singlet-level populations are given by the following simple steady-state equations:

$$F_2D_2 = F_4R_{42} + F_3R_{32}, \quad (8a)$$

$$F_3D_3 = F_4R_{43} + F_2R_{23} \quad (8b)$$

which, given Eq. (6), have the following solutions:

$$F_2 = \frac{P_4}{D_4D_2}\frac{R_{42}+R_{32}R_{43}/D_3}{1-R_{32}R_{23}/D_2D_3}, \quad (9a)$$

$$F_3 = \frac{P_4}{D_4D_3}\frac{R_{43}+R_{23}R_{42}/D_2}{1-R_{23}R_{32}/D_2D_3}. \quad (9b)$$

Equations (6), (9a), and (9b) exhibit all the important interactions and processes which control the presence or absence of gain in the Ne IX system. The fractional populations, hence gain, are all directly proportional to the pumping rate due to sodium photons P_4. The results for

gain given by Eqs. (6), (9a), and (9b) have been compared with the numerical results presented in Ref. 10 by using $T=227$ eV for P_4 in Eq. (5) and doubling the resulting value to account for the two-sided illumination assumed in Ref. 10. Generally good agreement is obtained with this previous work for the three strongest potential lasing lines ($2p\ ^1P_1-3d\ ^1D_2$, $2p\ ^1P_1-4d\ ^1D_2$, and $3d\ ^1D_2-4f\ ^1F_3$). The cutoff densities, above which lasing is impossible due to collisional spoiling of the inversion, are well represented by this analytic model. The densities of the lower states ($n=2$ and $n=3$ singlets) increase with R_{43} and R_{42} which in turn increase with electron density. Not surprisingly, all of the populations, hence the gain, are inversely proportional to the destruction rate D_4 of the $n=4$ singlets.

The results of Ref. 10 as well as the above analytic model have been developed under the assumption that the neon component of the plasma is optically thin. One of the most serious effects working against the practical achievement of gain in such a photon-pumped system is the potential presence of radiation trapping in the strong lines Ne IX $1s^2-1s2p\ ^1P$ and $1s^2-1s3p\ ^1P$. Such trapping will increase the populations of the $n=2$ and $n=3$ lower lasing states once the neon plasma becomes optically thick to these two lines. A neon plasma of characteristic width $w(\mu m)$ will reach optical depth of approximately unity in the $1s^2-1s2p\ ^1P$ line when $w\approx 5\times 10^{20}/N_e\ \mu m$. For the $1s^2-1s3p\ ^1P$ line the size would be 5.6 times greater before optical depth unity would be reached. The effect of radiation trapping on gain can be straightforwardly calculated with the above analytic model. The decay rates A_{21}, A_{31}, and A_{41} are replaced in Eqs. (7) by $A_{21}P_{e21}$, $A_{31}P_{e31}$, and $A_{41}P_{e41}$ where the P_e's are the spatially averaged photon-escape probabilities for the three resonance lines. For neon plasmas where significant gain is achievable (moderate optical depths and densities) a Doppler profile[13] provides an adequate P_e. In Fig. 1 are presented results for gain versus optical depth in the Ne IX 1-2 line. In this case a one-sided illumination with a sodium pump flux of 1330 ergs/cm^2 sec Hz is assumed. The neon plasma is assumed planar, as would be appropriate if either the target were planar or a thin shell of neon surrounded a cylinder or sphere containing the sodium pump. This is an effective pumping rate an order-of-magnitude smaller than that achieved in the Rochester experiment.[10,11] At $N_e=10^{19}$ cm^{-3} the gain exceeds 7 cm^{-1} in the 4-3 line up to optical depth 10. At $N_e=10^{20}$ cm^{-3} collisional mixing of the states has reduced the fractional inversion even for the optically thin case. Therefore, as the optical depth increases the gain in the 4-3 and 3-2 lines drops more sharply than in the corresponding lower-density case. The assumed neon-plasma temperature is 65 eV for these calculations. Direct attenuation of the pumping radiation is taken into account using the 1-4 optical depth from the center to the edge of the neon plasma. The gains at zero optical depth are an order-of-magnitude smaller than those of Ref. 10, exactly as expected for such a reduction in pump flux. Our assumed pumping flux of 1330 ergs/cm^2 sec Hz is readily achievable as is demonstrated below.

As seen from Fig. 1, radiation trapping will substantially reduce the gain although at $N_e=10^{19}$ cm^{-3}, neon plasmas of width $w=500$ μm could be tolerated before the gain drops to less than 7 cm^{-1} in the 4-3 line. One possibility for reducing this effect would be to intersperse the neon target with spatially discrete regions containing fluorine or a fluorine compound instead of neon. The hydrogenlike F IX line $1s$-$6p$ lies at 11.56 Å, compared to Ne IX $1s^2-1s3p\ ^1P$ which is at 11.544 Å. Thus the fluorine line could intercept the trapped 1-3 photons and possibly prevent their further diffusion in the neon plasma and subsequent repopulation of $n=3$. This scheme would not work if decay of F IX $n=6$ to $n=1$ always followed photoexcitation of $n=6$ by the trapped Ne IX photons. In that case the photons would re-enter the radiation field. However, once F IX $n=6$ is excited, decay to $n=1$ is very unlikely compared to the sum of the other possible processes such as radiative decay to $n=2$–5, and especially collisional transfer to $n=5$ and $n=7$. The overall fluorine quenching fraction for absorbed Ne IX photons is greater than 0.99 even at $N_e=10^{19}$ cm^{-3}. The major questions relating to this proposed technique are, can targets be designed to effectively intersperse sufficient absorbing fluorine in the neon plasma; and, also, would the F IX $1s$-$6p$ profile be sufficiently broadened by Stark and other effects to bridge the 16 mÅ gap between it and the trapped Ne IX $1s^2-1s3p\ ^1P$ line photons? A more definitive assessment is reserved for a future paper.

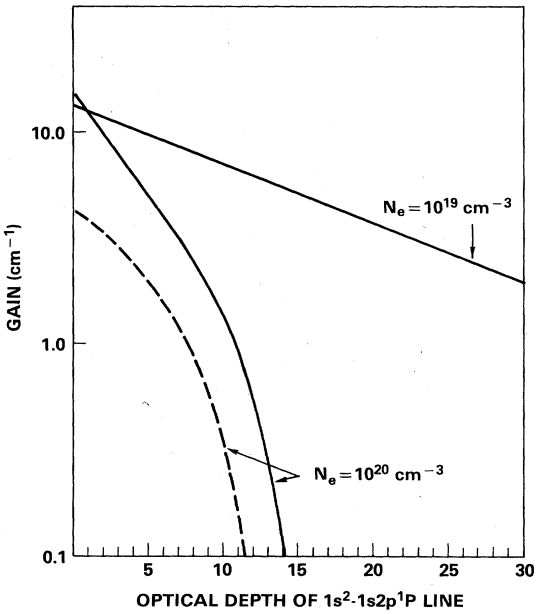

FIG. 1. Gain in the Ne IX $3d\ ^1D-4f\ ^1F$ (solid line) and $2p\ ^1P-3d\ ^1D$ (dotted line) lines is plotted against optical depth in the $1s^2-1s2p\ ^1P$ line. The planar neon plasma is assumed to have a temperature of 65 eV and is pumped on one side by a matched-line sodium flux of 1.3×10^3 ergs/cm^2 sec Hz.

III. SODIUM PUMPING POWER AS A FUNCTION OF PLASMA PROPERTIES

As has been detailed in Sec. II, the pumping power in Na X $1s^2-1s2p\ ^1P$ photons at 11.0027 Å is the principal

determinant of achievable gain in the neon laser-medium plasma. Therefore we turn our attention in this section to the question of the sensitivity of the pumping power to the basic properties of the sodium plasma—temperature, density, and size. To perform such an assessment we employ a numerical atomic model which assumes the sodium plasma to be in collisional-radiative equilibrium and includes radiation transport for all optically thick lines.

A. Atomic model and rates

We consider only sodium plasmas of such temperatures and densities that the K shell dominates the ionic species. Hence, only ground states are included in this model for all stages below lithiumlike. For the lithiumlike stages, the $1s^2 2s\ ^2S$ (ground), $1s^2 2p\ ^2P$, $1s^2 3s\ ^2S$, $1s^2 3p\ ^2P$, $1s^2 3d\ ^2D$, $1s^2 4l$, and $1s^2 5l$ levels are included. The heliumlike stage carries, in addition to the ground state, the $1s\,2s\ ^3S$, $1s\,2s\ ^1S$, $1s\,2p\ ^3P$, $1s\,2p\ ^1P$, $1s\,3l\ ^3L$, $1s\,3l\ ^1L$, $1s\,4l$, and $1s\,5l$ levels. The hydrogenlike levels include $n=1$—5.

The atomic processes populating and depopulating the levels are spontaneous radiative decay, electron collisional excitation and deexcitation, collisional ionization, and three-body, radiative, and dielectronic recombination. The continuum is optically thin in these plasmas; hence photoionization is neglected. Line photoexcitation is calculated by the radiative-transfer model discussed in the next section. The sources and calculational techniques used to obtain the rates are discussed elsewhere.[14]

B. Radiation transport

Continuum radiation is treated as optically thin, which is a good approximation for the plasmas considered below. Many lines are optically thick, however. For such lines, radiation transport is calculated self-consistently with the atomic-level populations for all of the optically thick lines which occur in the atomic model described above. For all of the sodium lines except the pumping $1s^2$—$1s\,2p\ ^1P$ line of the heliumlike stage, a probabilistic coupling-constant technique is used. This method has been presented in detail elsewhere,[13,15] hence, only a brief description is given here. For each of these lines a set of coupling constants is calculated which is a matrix of probabilities C_{ij} that if a photon is emitted in the ith spatial cell, it is absorbed in the jth cell. This calculation is based on simple but acceptably accurate expressions for the escape probability for a Voigt profile[16] as a function of optical depth. This technique accurately describes the photon pumping and escape, but since the escape factors are averaged over the line profile, the detailed frequency profile of the line emission is lost in this simplification.

For the pumping line Na X $1s^2$—$1s\,2p\ ^1P$ we need to know the detailed emitted profile to obtain the flux at the exact frequency where the pumped neon line occurs. Therefore, for this line only, a numerical frequency grid spanning the profile is established. Coupling constants are calculated at each frequency using the exponential escape probability which describes the transport of monochromatic radiation. Overall photon pumping is obtained by integrating over the line profile; since the emission at each frequency is known, the pumping flux at the neon line's frequency is obtainable. The iteration technique which is used to obtain self-consistency between the level populations and the radiation field is described in Ref. 17.

C. Numerical results

In a thermal plasma (Maxwellian particle distributions) the maximum attainable pumping flux at frequency ν is given by the Planck function. For the Na X $1s^2$—$1s\,2p\ ^1P$ line at 11.0027 Å this is given by Eq. (1):

$$\mathcal{F}_{\nu,\max} \approx 9.4\times 10^5 e^{-(1127\ \mathrm{eV})/T}\ \mathrm{ergs/cm^2\,sec\,Hz}\ , \quad (1')$$

where it is assumed that $\exp[(1127\ \mathrm{eV})/T] \gg 1$. To actually obtain the flux given by Eq. (1) from a plasma of kinetic temperature T(eV) requires that the plasma be in local thermodynamic equilibrium (LTE) and be optically thick in the line. To reach LTE requires either very high density, very high optical depth, or sufficient combination of high density and high optical depth. Note also that $\mathcal{F}_{\nu,\max}$ is a strongly increasing function of temperature in the 200—500 eV range where the heliumlike species of sodium ion predominates. Therefore, one expects that the pumping power would increase with density, size, and plasma temperature.

Quantitative results for such increases obtained with the numerical model described above are presented in Figs. 2 and 3. In Fig. 2 the emergent flux in the pumping line is plotted as a function of total ion density for an assumed cylindrical plasma diameter of 1.4 mm and temperature 400 eV. In Fig. 3 the same quantity is shown as a function of temperature with the ion density held constant at 10^{20} cm^{-3}. In Fig. 4 the flux is given as a function of plasma size with the temperature (400 eV) and ion density (10^{20} cm^{-3}) held constant. For Figs. 2 and 3, the

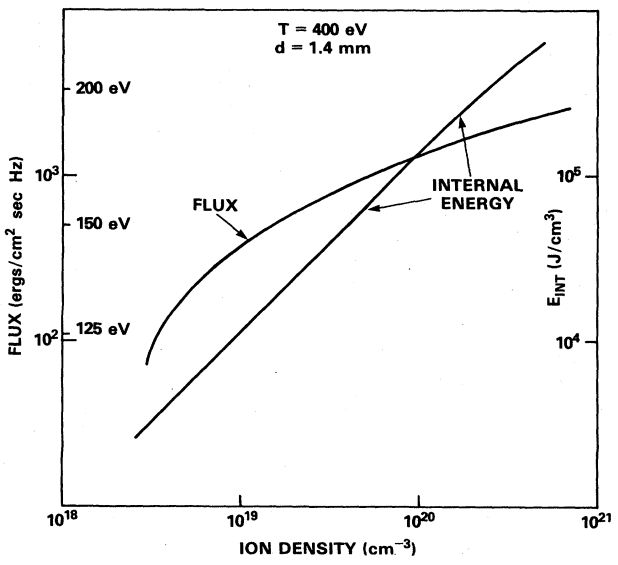

FIG. 2. Output flux in the Na X $1s^2$—$1s\,2p\ ^1P$ line at the frequency position of the pumped Ne IX $1s^2$—$1s\,4p\ ^1P$ line is shown as a function of ion density for a cylindrical plasma of temperature 400 eV and diameter 1.4 mm. Also shown is the internal energy per unit volume, as well as the equivalent blackbody brightness temperature of the emitted flux.

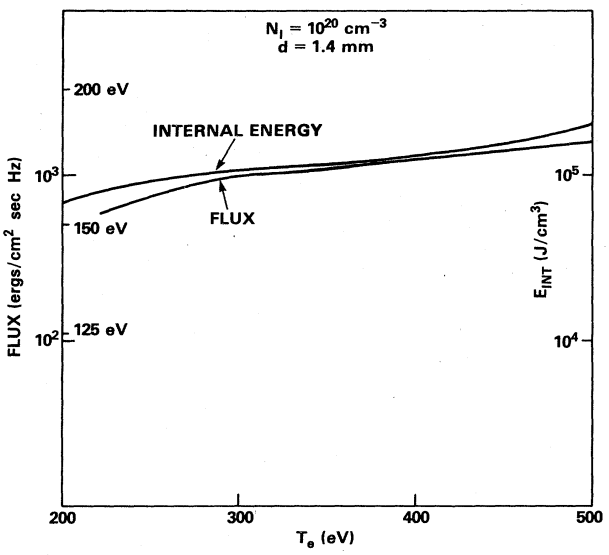

FIG. 3. Same as Fig. 2, except that the ion density is held constant at 10^{20} cm^{-3} and the quantities are plotted as a function of temperature.

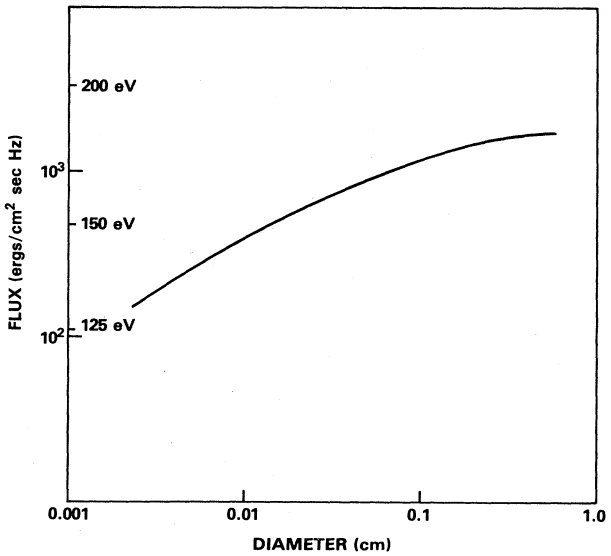

FIG. 4. Output flux in the Na X pumping line is given as a function of cylindrical-plasma diameter for a constant temperature of 400 eV and total ion density 10^{20} cm^{-3}.

plasma internal energy is also shown as a rough indication of the energetic price which must be paid by the experimenter to reach a given pumping power.

The pumping-line flux increases monotonically with temperature, density, and size, as expected. However, the growth is somewhat weaker than linear in these quantities, the strongest increase occurring as a function of density and the weakest as a function of temperature. The greatest pump flux calculated for a 400 eV, 1.4 mm plasma of ion density $\sim 10^{21}$ cm^{-3}, is 3×10^3 ergs/cm^2 sec Hz, about half that inferred from the Rochester pellet experiment.[10,11] Even at a diameter of 0.5 cm, Fig. 4 indicates that the pumping flux is more than an order-of-magnitude below the level of a 400 eV blackbody. The necessity for extremely high optical depth to achieve true LTE is detailed in Ref. 18. This flux is still quite adequate to pump neon, however. We have not carried our calculations to densities equivalent to those obtained at Rochester due to the uncertain effects of Stark broadening. Any pump flux above $\sim 10^3$ ergs/cm^2 sec Hz is sufficient to obtain gains exceeding 5 cm^{-1} in a properly prepared neon plasma.

Much insight into the functional behavior of the pumping power is obtained from studying the curves of Fig. 5. In Fig. 5 we display the fraction of all sodium ions in the heliumlike stage as a function of the same three basic plasma parameters—density, temperature, and size. Note that this fraction decreases monotonically as density, temperature, and size increase. The decrease with temperature is a straightforward consequence of the increasing ionization to the hydrogenlike and bare-nucleus stages. The pumping power is determined by the competition between the increasing collisional excitation rate for the $1s2p\ ^1P$ level and the decreasing fraction of ground-state ions available for excitation. As shown in Fig. 3, the increased collisional rate more than offsets—but barely—the reduction is ground-state ions. Thus the line intensity continues to increase with temperature.

The behavior with density and size is controlled by somewhat more subtle effects. As is evident from Fig. 5, the Na X heliumlike fraction decreases almost as strongly with increased size and density as it does with increased temperature. Also, the optical depth increases with both size and density, so surely more line photons are absorbed. Therefore, as before, the functional behavior of the line power output is governed by the interplay of increased total excitations in the plasma (due to increased size or density) and other factors. In this case the other factors are increased self-absorption and decreased ground-state fraction. The detailed behavior of these processes determines the resultant curves of Figs. 3 and 4, a slower-than-linear increase in power output with size and density.

The decrease in the heliumlike fraction with both density and size is perhaps surprising. It is due to the nature of the ionization process. At a temperature of 400 eV, the electron-impact ionization rate coefficient from the $1s^2\ ^1S_0$ ground state is 1.2×10^{-12} cm^3 sec^{-1}. From the $1s2p\ ^1P$ level the rate coefficient is 6.3×10^{-11} cm^3 sec^{-1}, and from the $n=5$ levels the rate coefficient exceeds 10^{-9} cm^3 sec^{-1}. Because the ionization rates are much higher from the excited states which lie much closer to the continuum, any process which increases the population of the excited levels will increase the ionization state of the plasma. Increasing the size of the plasma increases the excited-state populations through the increased photon pumping which results from greater optical depth. Increasing the density also increases the optical depth and photon pumping of the excited states, and an additional increase in the excited-state populations also occurs through the increase in collisional excitation. This accounts for the increased ionization and decreased heliumlike fraction with size and density shown in Fig. 5. We note that for a 1.4 mm sodium plasma of temperature 400

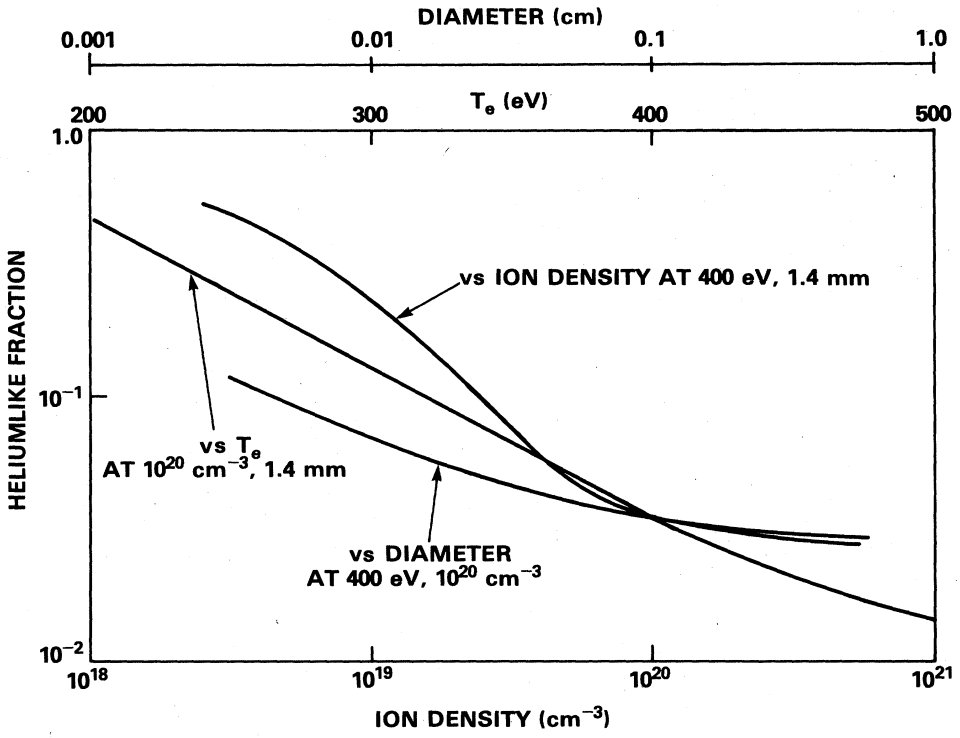

FIG. 5. The fraction of all sodium ions in the heliumlike stage is plotted as a function of ion density, plasma temperature, and plasma diameter. In each curve the remaining plasma parameters are held constant with the indicated values.

eV and ion density 10^{20} cm^{-3}, 80% of the ionization from the heliumlike to the hydrogenlike stage occurs from the excited states rather than the $1s^2\,{}^1S_0$ ground state. Even though size has no effect on the atomic rates, the increase in optical depth with size results in greater excited-state populations through photon pumping and greater ionization from the more highly populated excited-states. This underscores the importance of the excited-state populations to the overall ionization balance.

The transport of pump-line photons is clearly of great importance in determining the emitted-line power. In analyzing the transfer of line photons in laboratory plasmas, the following conceptual picture is often useful.[17] A line photon is "created" when the upper level of the transition is collisionally populated and then decays radiatively. Following its creation in an optically thick plasma the photon will generally be reabsorbed and reemitted a considerable number of times before ultimately escaping the plasma. During each reabsorption there is a finite probability P_Q that the level will be collisionally depopulated and the line photon destroyed. This probability P_Q is given by $D/(D+A)$ where D is the sum of the collisional rates out of the upper transition level, and A is the spontaneous decay rate for the line. Following the initial level excitation, collisional quenching or ultimate photon escape from the plasma will occur. We denote the probability of eventual escape by P_u; the probability of escape on any single flight is given by P_e. The quantity P_e is calculable given the optical depth and line profile; it is used, as described above, for calculating the coupling constants in radiative transfer. The quantity P_u may be obtained by considering the condition for a steady-state population density N of the upper level. Letting C stand for the collisional creation rate, this condition is

$$C = N(D + AP_e)\ \text{cm}^{-3}\,\text{sec}^{-1}\,, \tag{10}$$

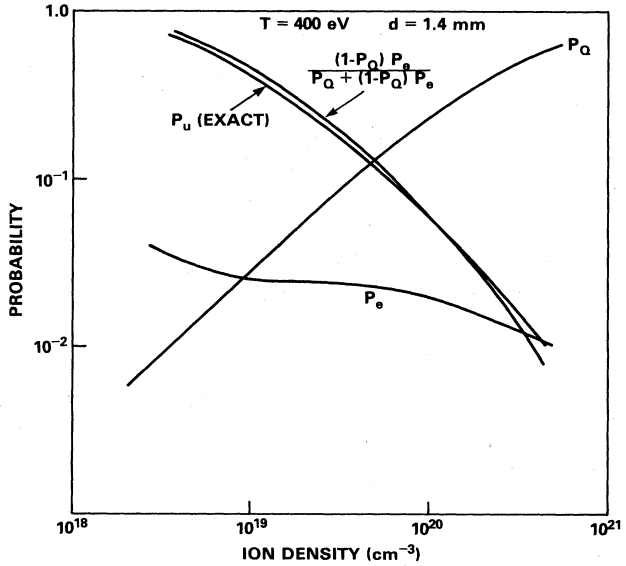

FIG. 6. The spatially averaged single-flight photon-escape probability P_e, the collisional photon-quenching probability per scattering P_Q, and the approximate analytic ultimate escape probability are plotted as a function of ion density for a 400 eV cylindrical sodium plasma of diameter 1.4 mm. Also shown is the exact computed numerical ultimate photon-escape probability P_u.

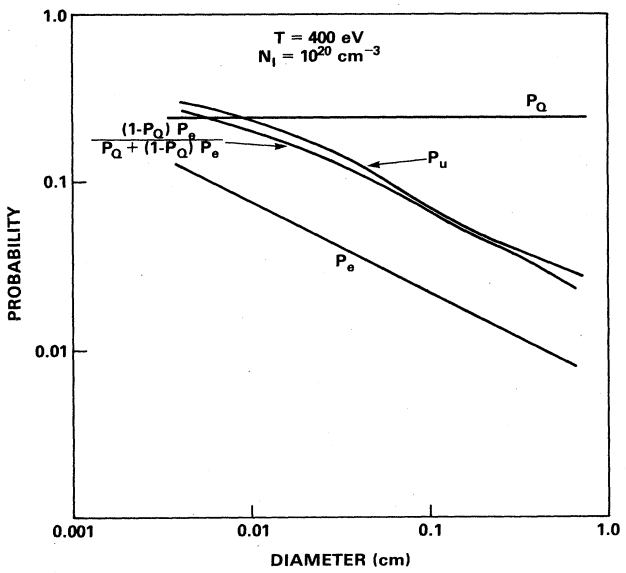

FIG. 7. Same as Fig. 6, except that the same quantities are plotted against plasma diameter for a total ion density of 10^{20} cm^{-3} at a temperature of 400 eV.

where in Eq. (10), radiative reabsorption of the line photons is taken into account by diluting the decay rate by the single-flight photon-escape probability. Even in a uniform plasma, P_e varies with position—Eq. (10) is intended as a spatially averaged approximate description of the photon transfer. After a few simple manipulations, Eq. (10) yields, taking into account that $P_Q = D/(A+D)$,

$$\frac{NAP_e}{C} = \frac{P_e(1-P_Q)}{P_Q+(1-P_Q)P_e} . \tag{11}$$

However, the left-hand side of Eq. (11) is the total photon emission divided by the total upper-level excitation rate; that is, precisely the ultimate escape probability. Therefore,

$$P_u = \frac{P_e(1-P_Q)}{P_Q+(1-P_Q)P_e} \tag{12}$$

in this approximation.

In Figs. 6 and 7 we have plotted the quantities P_e, P_Q, and $P_e(1-P_Q)/[P_Q+(1-P_Q)P_e]$ versus sodium ion density and diameter, respectively. These parameters are displayed for the Na X $1s^2-1s\,2p\ ^1P$ line for a temperature of 400 eV and, for Fig. 6, a fixed diameter of 1.4 mm. Figure 7 reflects calculations for a fixed sodium ion density of 10^{20} cm^{-3}. P_e and P_Q are obtained from Voigt profile formulas and the atomic rates, respectively. The accuracy of the spatial-average approximation is indicated in both Figs. 6 and 7 by also plotting P_u as numerically calculated from the actual computed line photon output power. As is obvious, excellent correspondence is obtained with the probabilistic, spatial-average approximation of Eq. (12). This is especially significant in light of the fact that even though the plasma temperature and density are assumed spatially uniform, the presence of a boundary ensures a significant degree of nonuniformity in both the photon field and the spatial profile of the level populations.

The important feature of Figs. 6 and 7 relevant to the line power output is the monotonic decrease of the ultimate photon-escape probability P_u with density and plasma size. Together with the decreasing heliumlike ionic fraction, this increased photon absorption results in the relatively weak pump power increase with size and density. Were the ionization and reabsorption phenomena not present, the pumping power would increase as the square of the density and linearly with the diameter of a cylindrical plasma. The ultimate escape probability P_u is seen from Figs. 6 and 7 to decrease faster with density than with size. This is a consequence of the fact that as size increases, only P_e, the single-flight escape probability, decreases if the density is constant. As the density increases, P_e decreases and P_Q increases which, according to Eq. (12), results in a faster decrease of P_u.

IV. CONCLUDING REMARKS

The most important plasma atomic processes which determine the viability of resonantly photoexcited x-ray laser schemes have been investigated in detail with both analytic and numerical models. The well-known and promising Na X—Ne IX system was chosen for specific analysis, although the general trends discovered would be valid for similar matched-line schemes.

For the pumped neon plasma, the rate and level kinetics which determine the presence or absence of gain in the lasing lines were shown to be amenable to an accurate analytic treatment which displays in a few simple equations all the important dependencies. The technique is also capable of calculating the deleterious effects of radiation trapping on achievable gain. We suggest that use of fluorine in the neon plasma may assist in removing photons trapped in the $1s^2-1s\,3p\ ^1P$ line thereby counteracting some of the unwanted effects.

For the pumping sodium plasma, the behavior of the power output in the pumping line Na X $1s^2-1s\,2p\ ^1P$ has been quantified as a function of plasma size, temperature, and density. The functional behavior is explained as resulting from the interplay of increased collisional excitation and photon reabsorption with decreased heliumlike ionic fraction. The photon transport has also proven amenable to an analytic treatment in which the ultimate photon-escape probability is given in terms of a single-flight photon-escape probability and collisional quenching parameter.

Another result of the investigation has been the determination that two physically separate neon- and sodium-plasma components are required for significant gain. Numerical calculations have shown that mixing the sodium and neon ions cannot produce conditions conducive to lasing. When the mixture is hot and dense enough to produce adequate sodium pump radiation the neon is overionized well past the heliumlike stage. This occurs

because pumping of the $1s\,4p\ ^1P$ level in Ne IX greatly facilitates ionization. Conversely, a mixture cool enough and tenuous enough for proper lasing conditions does not produce enough pumping radiation. The scheme appears to be very promising, however, if spatially separate sodium and neon components are used.

ACKNOWLEDGMENTS

The authors have appreciated the invaluable assistance with the atomic rates and coding provided by D. Duston and C. Agritellis. This work was supported by the U.S. Defense Advanced Research Projects Agency.

[1]A. V. Vinogradov, I. I. Sobelman, and E. A. Yukov, Kvant. Elektron. (Moscow) **2**, 105 (1975) [Sov. J. Quantum Electron. **5**, 59 (1975)].
[2]B. A. Norton and N. J. Peacock, J. Phys. B **8**, 989 (1975).
[3]V. A. Bhagavatula, Appl. Phys. Lett. **33**, 726 (1978).
[4]V. A. Bhagavatula, IEEE J. Quantum Electron. **16**, 603 (1980).
[5]J. Trebes and N. Krishnan, Phys. Rev. Lett. **50**, 679 (1983).
[6]P. L. Hagelstein, University of California Report No. UCRL-53100, 1981 (unpublished).
[7]W. E. Alley, G. Chapline, P. Kunasz, and J. C. Weisheit, J. Quant. Spectrosc. Radiat. Transfer **27**, 257 (1982).
[8]P. G. Burkhalter, G. Charatis, and P. D. Rockett, J. Appl. Phys. **54**, 6138 (1983).
[9]R. H. Dixon and R. C. Elton, J. Opt. Soc. Am. B **1**, 231 (1984).
[10]J. P. Apruzese, J. Davis, and K. G. Whitney, J. Appl. Phys. **53**, 4020 (1982).
[11]B. Yaakobi, D. Steel, E. Thoros, A. Hauer, and B. Perry, Phys. Rev. Lett. **39**, 1526 (1977).
[12]F. L. Cochran, J. Davis, and J. P. Apruzese, J. Appl. Phys. **57**, 27 (1985).
[13]J. P. Apruzese, J. Quant. Spectrosc. Radiat. Transfer **25**, 419 (1981).
[14]D. Duston, J. Davis, and C. Agritellis, J. Appl. Phys. **57**, 785 (1985).
[15]J. P. Apruzese, J. Davis, D. Duston, and K. G. Whitney, J. Quant. Spectrosc. Radiat. Transfer **23**, 479 (1980).
[16]J. P. Apruzese (unpublished).
[17]J. P. Apruzese, J. Davis, D. Duston, and R. W. Clark, Phys. Rev. A **29**, 246 (1984).
[18]J. P. Apruzese, P. C. Kepple, K. G. Whitney, J. Davis, and D. Duston, Phys. Rev. A **24**, 1001 (1981).